Geoscience Frontiers 7 (2016) 937–951

Contents lists available at ScienceDirect

China University of Geosciences (Beijing)

Geoscience Frontiers

journal homepage: www.elsevier.com/locate/gsf

Research paper

Cretaceous alkaline volcanism in south Marzanabad, northern central Alborz, Iran: Geochemistry and petrogenesis

Roghieh Doroozi [a,*], Carmela Vaccaro [b], Fariborz Masoudi [a], Riccardo Petrini [c]

[a] Faculty of Earth Science, Shahid Beheshti University, Velenjak, Tehran, Iran
[b] Department of Mineralogy, University of Ferrara, Corso Ercole I d'Este 32, 44100 Ferrara, Italy
[c] Department of Mathematics and Geosciences, University of Trieste, Via Weiss, 8-34100 Trieste, Italy

A R T I C L E I N F O

Article history:
Received 8 June 2015
Received in revised form
6 October 2015
Accepted 4 November 2015
Available online 30 November 2015

Keywords:
Volcanic rocks
Cretaceous
Marzanabad
Central Alborz
Iran

A B S T R A C T

The alkali-basalt and basaltic trachy-andesites volcanic rocks of south Marzanabad were erupted during Cretaceous in central Alborz, which is regarded as the northern part of the Alpine-Himalayan orogenic belt. Based on petrography and geochemistry, en route fractional crystallization of ascending magma was an important process in the evolution of the volcanic rocks. Geochemical characteristics imply that the south Marzanabad alkaline basaltic magma was originated from the asthenospheric mantle source, whereas the high ratios of $(La/Yb)_N$ and $(Dy/Yb)_N$ are related to the low degree of partial melting from the garnet bearing mantle source. Enrichment pattern of Nb and depletion of Rb, K and Y, are similar to the OIB pattern and intraplate alkaline magmatic rocks. The K/Nb and Zr/Nb ratios of volcanic rocks range from 62 to 588 and from 4.27 to 9 respectively, that are some higher in more evolved samples which may reflect minor crustal contamination. The isotopic ratios of Sr and Nd respectively vary from 0.70370 to 0.704387 and from 0.51266 to 0.51281 that suggest the depleted mantle as a magma source. The development of south Marzanabad volcanic rocks could be related to the presence of extensional phase, upwelling and decompressional melting of asthenospheric mantle in the rift basin which made the alkaline magmatism in Cretaceous, in northern central Alborz of Iran.

1. Introduction

Plutonic or volcanic alkaline rocks are typically associated with continental rifting or intraplate continental and oceanic settings that typically related to the partial melting of asthenospheric mantle (McKenzie and Bickle, 1988; White and McKenzie, 1989; Wilson and Downes, 1991; Ernst et al., 2005; Ganguly, 2005; Lustrino and Carminati, 2007).

Fractional crystallization, magma mixing and crustal contamination are the main processes in the evolution of magmas (Best, 1970; Wilson, 1989; Hall, 1996; Rollinson, 1998; McBirney, 2006). The effect of these processes in magmatism in orogenic belts, could be cleared by geochemistry and petrology studies.

Marzanabad area in northern part of central Alborz is a part of Alpine-Himalayan orogenic that formed in Cretaceous with well developed sub-marine alkaline volcanic sequences. The volcanism associated with Barremian–Aptian and Cenomanian limestone layers clarified Cretaceous age for volcanic rocks (Cartier, 1971; Sussli, 1976; Vahdati Daneshmand and Nadim, 2001), while there are no corresponding radiometric ages available.

In Marzanabad area, the outcrops of volcanic rocks, allow us to investigate the Cretaceous volcanism of Alpine Himalayan orogenic belt in Iran. Little is known on Paleozoic and Mesozoic igneous activity in central Alborz, whereas only few aspects are known for the Cenozoic activity. However, neither whole-rock geochemistry nor microprobe or isotopic data have been published for the volcanic rocks of Marzanabad area. In this study, major and trace element, microprobe and Sm-Nd isotopic data are used to constrain the role of fractional crystallization and mantle source in the petrogenesis of alkaline magma from Marzanabad area, central Alborz.

* Corresponding author. Tel.: +98 2155020028, +98 9124930570 (mobile); fax: +98 2165573318.
E-mail address: r.doroozi220@gmail.com (R. Doroozi).
Peer-review under responsibility of China University of Geosciences (Beijing).

http://dx.doi.org/10.1016/j.gsf.2015.11.004
1674-9871/

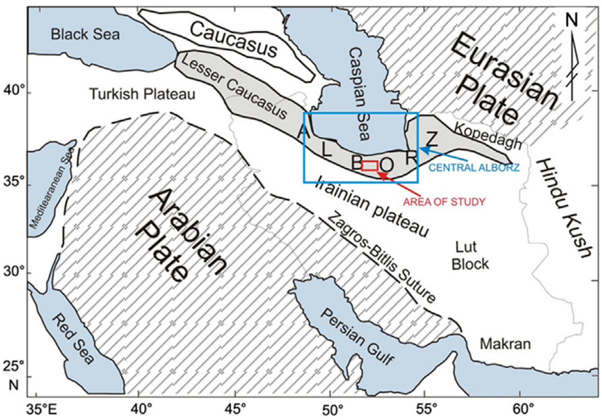

Figure 1. General tectonic map of Iran with Arabian and Eurasian plate and the location of studied area in central Alborz zone.

Results of this study may help to have a better understanding of Cretaceous alkaline magmatism that produced the alkaline volcanic rocks in Alpine Himalayan orogenic belt in central Alborz.

2. Geodynamics background

Central Alborz was a part of the Gondwana plate in early Paleozoic. It separated from Gondwana during Ordovician to Silurian and then collided with Eurasian plate in Triassic, causing the Paleotethys Ocean closure to the north, and the formation of the Neotethys Ocean to the south (Stocklin, 1974; Berberian and King, 1981; Stampfli et al., 1991). After the Triassic collisional event, along both sides of the Paleotethys Ocean, intracontinental compressions were initiated and accompanied by deposition of coal bearing Shemshak Jurassic formation (Berberian, 1983). Compressional tensions coupled with some regional extensional pressures, which were caused by the convergence of Arabian and Eurasian plates (Zanchi et al., 2006).

In central Alborz, Mesozoic era began with the deposition of detrital carbonate sediments which is continued with deposition of Shemshak Formation in late Triassic. In the studied area, extensional phases were started in upper Triassic associated with alkaline igneous activity. This alkaline magmatic phase can be assumed as an evidence for intracontinental tectonic setting related to a rift system in central Alborz during late Triassic (Furon, 1941; Steiger, 1966; Taraz, 1974; Annells et al., 1975; Nabavi and Seyed emami, 1977; Kristan-Tollmann et al., 1979; Berberian and King, 1981; Berberian, 1983; Völlmer, 1987; Fauvelet and Eftekhar Nezhad, 1992; Sabzehei, 1993; Brunet et al., 2003; Seyed emami, 2003; Shahidi, 2005, 2008; Nazari and Shahidi, 2011).

In central Alborz, extensional movements started at the same time with Rhaetic rift volcanism and deposition of coal-bearing Shemshak Formation, in Mesozoic era (Berberian, 1983; Nazari et al., 2004). The extensional phases developed some regional rifts which caused volcanism and plutonism activities in central Alborz (Berberian, 1983).

Soffel and Förster (1984) believed that the extensional movements lead to separation of the central Iranian plate from Eurasia plate, during Jurassic. Lithospheric ruptures, tensions and extensions with ascending of asthenospheric plumes and their partial melting caused the development of the rift system in Alborz zone from middle Jurassic to lower Cretaceous. Extension and the rift development could not persist more than few million years since the tectonical movements of Maastrichtian (Laramide) terminated the extension period.

3. Regional geology

Alborz Mountains are a geological structural zone in north of Iran considered as part of the northern margin of the Alpine-Himalayan orogenic belt (Fig. 1). Alborz block is connected to Caucasus Mountains in the northwest and is bounded by Hindu Kush Mountains in the east (Zanchi et al., 2006), that was part of the Gondwana plate in early Paleozoic. During Ordovician to Silurian, Alborz separated from Gondwana and finally collided with the

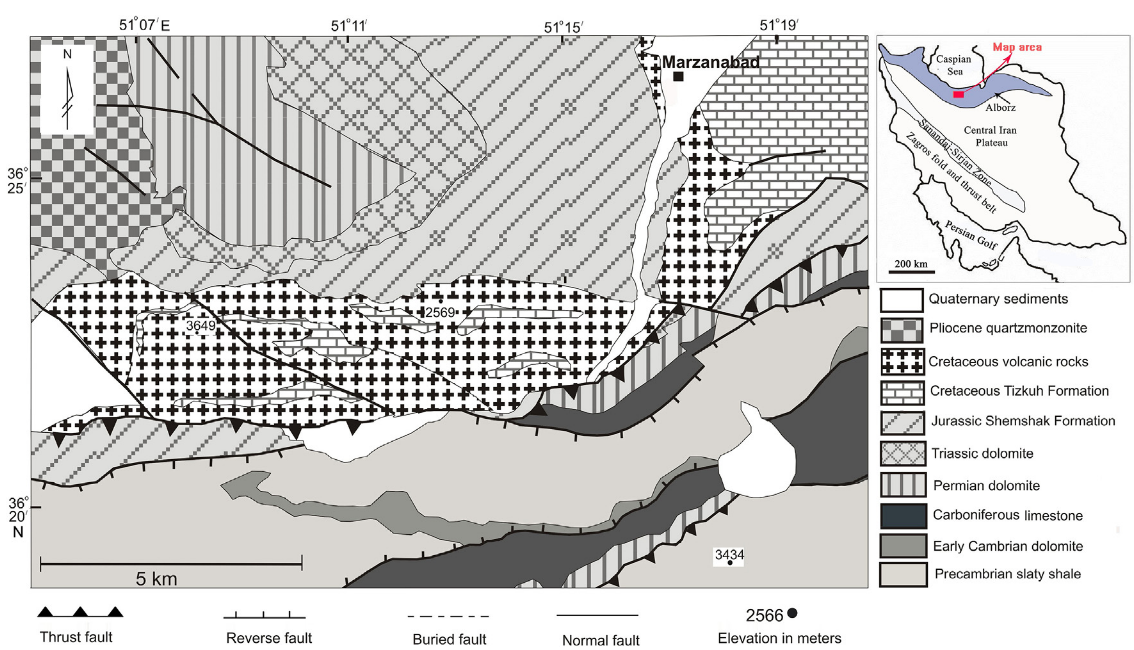

Figure 2. Geological map of the study area with the position of analyzed samples. Modified from the 1:100,000 Marzanabad geological map of Iran.

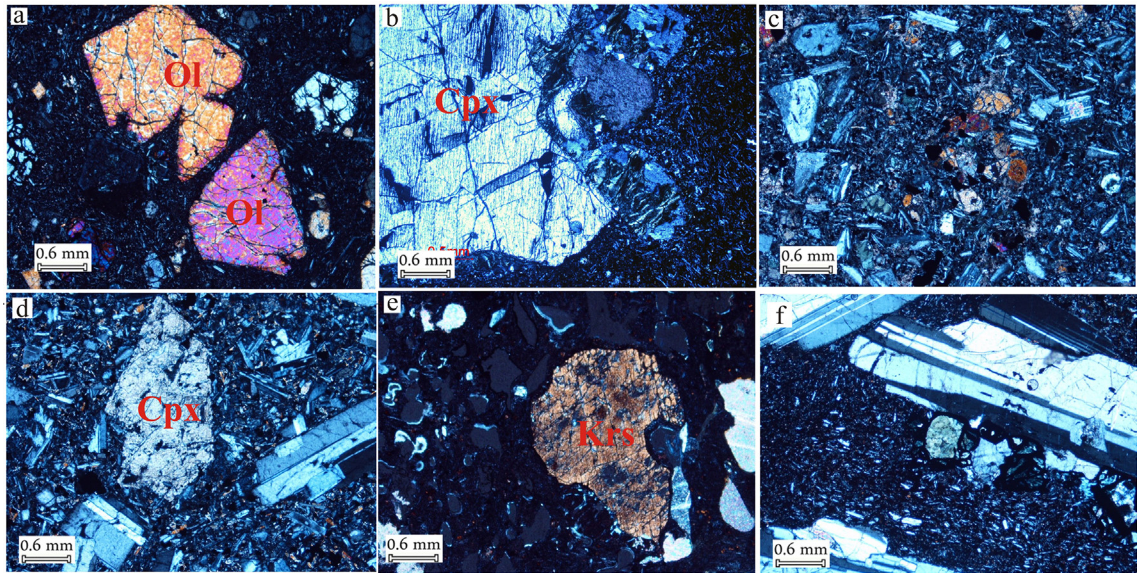

Figure 3. (a) Phenocrysts of olivine (Ol) in alkali-olivine basalts; (b) megacryst of pyroxene (Cpx) in alkali-olivine basalts; (c) glomeroporphyric texture in Cpx of alkali-basalts; (d) phenocrysts of Cpx and plagioclase in basaltic trachy-andesites; (e) kaersutite (Krs) amphibole in basaltic trachy-andesites; (f) megacryst of plagioclase in basaltic trachy-andesite rock.

Eurasia plate in Triassic (Alavi, 1991; Stampfli, 1996, 2000). So, the Alborz block can be considered as an active mountain belt which is the consequence of Gondwana and Eurasia plate collision in Triassic (Stocklin, 1974; Berberian and King, 1981; Sengör et al., 1988; Sengör, 1990; Stampfli et al., 1991; Sengör and Natalin, 1996; Guest et al., 2006). In Paleozoic and early Mesozoic, regional extensional events are reported by different studies in all basement of Iran including Alborz block, central Iranian plateau, Kopeh Dagh zone, Zagros zone, Lut block and Sanandaj-Sirjan zone (Berberian, 1979; Berberian and King, 1981; Berberian et al., 1982; Zanchi et al., 2006).

During Mesozoic in central Alborz, extensional phases are started along with the occurrence of upper Triassic rift volcanism (Rhaetic) and deposition of shaly, coal-bearing Shemshak Formation by the Triassic collision between Arabian and Eurasian plates (Berberian et al., 1982). During upper Jurassic and lower Cretaceous, in the study area, shallow marine limestones deposited and accompanied with eruptions of alkaline basalts (Barrier and Vrielynck, 2008; Nazari and Shahidi, 2011).

The study area is located in the northern part of Alborz structural zone that is called central Alborz (Fig. 1). Central Alborz is composed of Paleozoic to Quaternary sedimentary rocks, wide range of Paleozoic to Quaternary volcanic rocks and some outcrops of metamorphic rocks in the northern border line. Intrusions are also common in this area, with the probably age of Paleocene and Oligocene (Fig. 2).

Table 1
Representative microprobe analysis of olivines in south Marzanabad volcanic rocks (oxides are in wt.% and elements are in apfu). Calculation is based on four oxygen.

Sample	CA53	CA53	CA53	CA53	CA53	CA53	CA53	CA53	CA53	CA53	CA53	CA53
Note	Core	Core	Core	Rim	Rim	Rim	Rim	Core	Rim	Core	Core	Core
Na_2O	0	0	0.01	0	0.02	0	0.02	0	0	0	0.01	0.02
MgO	37.17	38.27	36.68	34.61	33.68	42.8	44.13	44.25	43.48	44.38	46.56	47.41
Al_2O_3	0.04	0.1	0.02	0.01	0	0.06	0.04	0.06	0.03	0.07	0	0.03
SiO_2	37.13	37.16	37.11	36.68	36.36	38.62	38.45	38.72	38.81	39.34	40.01	40.27
CaO	0.31	0.34	0.3	0.31	0.45	0.31	0.24	0.23	0.21	0.12	0.27	0.25
TiO_2	0.05	0.07	0.04	0.03	0.06	0	0.02	0.01	0	0	0.02	0
Cr_2O_3	0.02	0.03	0.02	0	0	0.02	0.01	0	0.02	0.02	0.1	0.04
MnO	0.43	0.37	0.48	0.58	0.56	0.29	0.2	0.23	0.29	0.21	0.15	0.21
FeO	25.82	24.02	25.83	28.69	28.98	18.09	17.47	16.56	17.02	16.85	13.27	12.44
Total	100.97	100.5	100.76	101.15	100.17	100.27	100.65	100.06	99.86	100.99	100.38	100.67
Si	0.98	0.97	0.98	0.98	0.98	0.98	0.97	0.98	0.99	0.99	0.99	0.99
Ti	0	0	0	0	0	0	0	0	0	0	0	0
Al	0	0	0	0	0	0	0	0	0	0	0	0
Cr	0	0	0	0	0	0	0	0	0	0	0	0
Fe^{2+}	0.57	0.53	0.57	0.64	0.65	0.39	0.37	0.35	0.36	0.35	0.28	0.26
Mn	0.01	0.01	0.01	0.01	0.01	0.01	0	0	0.01	0	0	0
Mg	1.46	1.5	1.44	1.38	1.35	1.63	1.67	1.67	1.65	1.66	1.72	1.74
Ca	0.01	0.01	0.01	0.01	0.01	0.01	0.01	0.01	0.01	0	0.01	0.01
Na	0	0	0	0	0	0	0	0	0	0	0	0
Ni	0	0	0	0	0	0	0	0	0	0	0	0
Total	3.02	3.02	3.02	3.02	3.02	3.01	3.03	3.02	3.01	3.01	3.01	3.01
Fo	71.62	73.66	71.3	67.82	67.01	80.58	81.65	82.45	81.75	82.26	86.08	86.98
Fa	27.91	25.94	28.17	31.54	32.35	19.11	18.13	17.31	17.95	17.52	13.76	12.8
$Mg^{\#}$	71.96	73.96	71.68	68.26	67.45	80.83	81.83	82.65	82	82.44	86.22	87.17

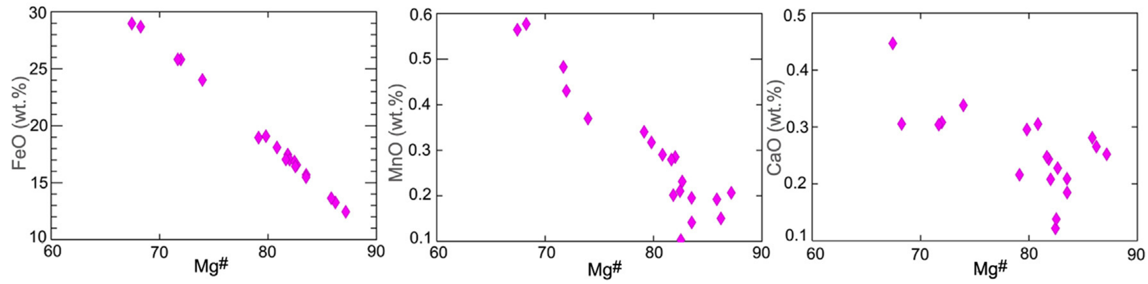

Figure 4. FeO, MnO and CaO versus $Mg^{\#}$ in the olivines of south Marzanabad volcanic rocks.

A sequence of Precambrian to Cretaceous sedimentary rocks with some unconformities and hiatuses are observed in the study area. In 1971 Cartier suggested a collection of Cretaceous carbonate sediments and volcanic rocks as Chalus Formation in north Marzanabad that locates on Jurassic Shemshak Formation with angular unconformity. Cartier (1971) regarded 5 members for this formation. The first member consists of lower Cretaceous basic volcanic rocks which covered by the Tizkouh Formation (Aptian–Cenomanian orbitolina-enriched limestone). However, volcanic rocks which covered the Tizkouh Formation belong to upper Cretaceous and include other members of Chalus Formation (Cartier, 1971). In some places, limestone layers with large amount of Orbitolina and other Cenomanian–Coniacian fossils, are observed among volcanic rocks (Vahdati Daneshmand and Nadim, 2001).

4. Analytical methods

Samples with the most possible fresh chips were selected and powdered in an agate mill. X ray fluorescence (XRF) for major and some trace elements (Ni, Co, Cr, V, Sr, Ba and Rb) was analyzed on powder pellets, using a wavelength-dispersive automated Philips PW 1400 spectrometer at the Department of Earth Sciences (Ferrara University), based on the method by Franzini et al. (1975) and Leoni and Saitta (1975). Trace and rare-earth elements were analyzed by inductively coupled plasma mass spectrometry (ICP-MS) at the same place, using a VG Plasma Quad2 plus. Mineral compositions were measured at the Department of Mineralogy (Padua University) with a Cameca–Camebax electron microprobe (fitted with three spectrometers) at accelerating voltage of 15 kV, and specimen current of 15 nA, using natural silicates and oxides as standards. The beam was enlarged to a diameter of 5 μm and the counting times were set to 10 s for both peak and background and the data correction was performed using PAP methods (Pouchou and Pichoir, 1984).

Isotopic analyses on whole rocks were carried out at the Department of Mathematics and Geosciences (Trieste University); whole-rock was leached with hot 6 N HCl and then digested with $HF\text{-}HNO_3$. Strontium and REE were separated by using standard

Table 2
Representative microprobe analysis of pyroxenes in south Marzanabad volcanic rocks (oxides are in wt.% and elements are in apfu). Calculation is based on six oxygen.

Sample	RD29	RD2	RD29	CA53	CA53	CA53	RD107	RD107	RD107	RD107	RD107	RD107
Note	Rim	Middle	Core	Core	Middle	Rim	Core	Middle	Rim	Core	Middle	Rim
Na_2O	0.43	0.4	0.43	0.59	0.59	0.52	0.29	0.37	0.37	0.35	0.45	0.6
MgO	15.15	14.96	15.13	13.07	13.19	12.93	14.57	13.65	12.25	13.85	13.15	11.66
Al_2O_3	6.42	6.54	6.31	8.56	8.28	6.08	3.86	3.33	6.92	3.25	2.7	2.25
SiO_2	49.19	48.85	48.61	44.94	45.83	46.35	48.45	49.45	45.54	49.75	49.77	47.77
K_2O	0.01	0.01	0	0	0.01	0	0	0	0	0	0	0
CaO	21.23	21.05	21.18	21.67	22.08	22.32	21.33	21.44	21.82	22	21.94	22.09
TiO_2	0.84	0.82	0.79	2.57	2.44	2.63	1.53	1.63	2.84	1.82	1.95	1.72
Cr_2O_3	0.53	0.66	0.62	0.81	0.79	0.35	0.03	0.05	0	0	0.04	0.03
MnO	0.13	0.14	0.17	0.11	0.1	0.13	0.2	0.21	0.2	0.2	0.21	0.23
FeO	5.96	5.93	5.9	6.25	6	6.66	8.64	9.24	8.95	8.29	9.39	12.6
Total	99.9	99.36	99.16	98.56	99.29	97.97	98.9	99.37	98.89	99.51	99.6	98.97
Si	1.8	1.8	1.8	1.68	1.7	1.75	1.82	1.86	1.72	1.86	1.87	1.82
Ti	0.02	0.02	0.02	0.07	0.07	0.07	0.04	0.05	0.08	0.05	0.06	0.05
Al	0.28	0.28	0.27	0.38	0.36	0.27	0.17	0.15	0.31	0.14	0.12	0.1
Cr	0.02	0.02	0.02	0.02	0.02	0.01	0	0	0	0	0	0
Fe^{3+}	0.09	0.08	0.1	0.13	0.11	0.1	0.13	0.08	0.12	0.06	0.06	0.19
Fe^{2+}	0.1	0.11	0.08	0.07	0.07	0.11	0.14	0.21	0.17	0.2	0.23	0.21
Mn	0	0	0.01	0	0	0	0.01	0.01	0.01	0.01	0.01	0.01
Mg	0.83	0.82	0.83	0.73	0.73	0.73	0.81	0.76	0.69	0.77	0.74	0.66
Ca	0.83	0.83	0.84	0.87	0.88	0.91	0.86	0.86	0.88	0.88	0.88	0.9
Na	0.03	0.03	0.03	0.04	0.04	0.04	0.02	0.03	0.03	0.03	0.03	0.04
Total	4	4	4	4	4	4	4	4	4	4	4	4
Al^{IV}	0.2	0.2	0.2	0.32	0.3	0.25	0.17	0.14	0.28	0.14	0.12	0.1
Al^{VI}	0.08	0.09	0.07	0.06	0.07	0.03	0	0	0.03	0	0	0
$Mg^{\#}$	89.42	88.38	91.37	91.62	90.86	86.48	83.05	78.02	80.52	79.37	74.31	65.06
Ti/Al	0.08	0.08	0.08	0.19	0.19	0.28	0.25	0.31	0.26	0.36	0.46	0.49
Wo	0.47	0.48	0.48	0.52	0.52	0.52	0.47	0.51	0.48	0.48	0.51	0.5
Fs	0.06	0.05	0.05	0.04	0.07	0.06	0.12	0.1	0.11	0.13	0.12	0.14
En	0.47	0.48	0.47	0.43	0.42	0.42	0.42	0.4	0.42	0.4	0.37	0.37

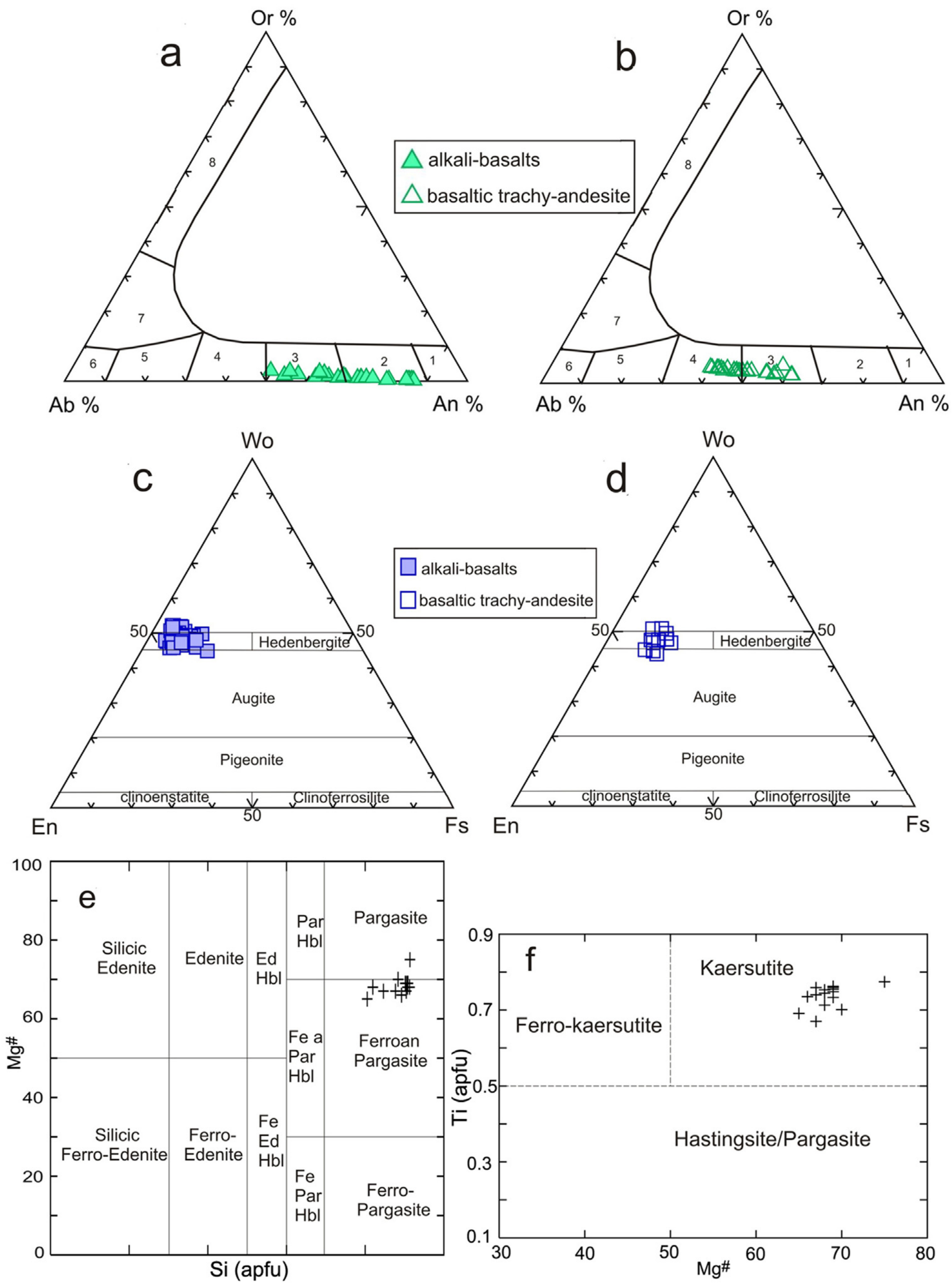

Figure 5. (a, b) Pyroxene composition of the south Marzanabad volcanic rocks in the ternary classification diagram from Morimoto et al. (1988). 1–Anorthite, 2–Bytonite, 3–Labradorite, 4–Andesine, 5–Oligoclase, 6–Albite, 7–Anorthoclase, 8–Sanidine. (c, d) Plagioclases composition of south Marzanabad volcanic rocks in the ternary diagram. (e, f) Composition of amphiboles in south Marzanabad basaltic trachy-andesite rocks which represents pargasite, ferroan pargasite and kaersutite composition (Leake et al., 1997).

cation exchange chromatographic columns with an AG 50W-X8 resin using 2.5 N HCl for Sr and 6 N HCl for the REE. Nd was separated from the other REE by using HDEHP-coated Teflon columns and 0.12 N HCl. The Sr and Nd isotope ratios were corrected by normalizing to $^{86}Sr/^{88}Sr = 0.1194$ and $^{146}Nd/^{144}Nd = 0.7219$ and using standards SRM 987 and JNdi-1 for Sr and Nd, respectively.

5. Petrography

Based on petrographical studies, south Marzanabad volcanic rocks are classified into two groups: alkali-basalts and basaltic trachy-andesites.

5.1. Alkali-basalts

Alkali-basalts are dark gray to dark green in hand specimen and show massive structures. The rocks are mainly alkali-basalts and alkali-olivine basalts with mostly porphyritic texture. Phenocrysts of alkali-olivine basalts are olivine, pyroxene and minor plagioclase, while the matrix consists of pyroxene, plagioclase and accessory apatite and opaque oxide minerals (Fig. 3a). Olivine phenocrysts mostly altered to iddingsite. Porphyritic alkali-basalts contain pyroxene and plagioclase as phenocrysts with glomeroporphyric texture in some pyroxenes (Fig. 3b,c). Matrix of Alkali-basalts contains plagioclase and pyroxene with apatite, alkali feldspar and opaque accessory minerals.

Table 3
Representative microprobe analysis of plagioclases in south Marzanabad volcanic rocks (oxides are in wt.% and elements are in apfu). Calculation is based on 8 oxygen.

Sample	RD109	RD109	RD109	RD109	RD150	RD150	RD107	RD107	RD107	CA24	CA24	CA24
Note	Core	Rim	Core	Core	Rim	Core	Middle	Middle	Core	Core	Core	Rim
Na_2O	1.48	3.8	1.64	3.5	5.33	3.59	6.18	5.66	4.14	5.72	6.08	6.27
MgO	0.05	0.1	0.08	0.1	0.06	0.07	0.05	1.03	0.11	0.03	0.01	0.02
Al_2O_3	33.67	29.86	32.97	30.57	28.01	30.39	26.55	25.29	29.52	27.57	26.99	26.2
SiO_2	45.6	51.14	46.26	50.19	54.84	49.99	56.68	54.61	52.14	55.51	56.32	56.69
K_2O	0.03	0.24	0.07	0.16	0.5	0.17	0.72	0.67	0.39	0.61	0.73	0.78
CaO	17.51	13.24	16.82	14.1	10.12	13.84	8.61	8.25	12.48	9.54	8.64	8.14
TiO_2	0.02	0.15	0.03	0.06	0.15	0.1	0.07	0.05	0.14	0.07	0.08	0.04
Cr_2O_3	0	0	0.02	0.01	0.02	0.01	0.03	0.02	0.05	0.02	0	0
MnO	0	0.01	0	0	0	0.04	0	0.05	0	0	0.01	0.01
FeO	0.44	0.82	0.45	0.71	0.53	0.54	0.3	1.66	0.57	0.25	0.19	0.28
Total	98.78	99.2	98.32	99.35	99.4	98.62	99.12	97.23	99.41	99.26	98.98	98.38
Si	2.13	2.35	2.16	2.31	2.49	2.31	2.57	2.54	2.38	2.52	2.56	2.59
Ti	0	0.01	0	0	0.01	0	0	0	0	0	0	0
Al	1.85	1.62	1.82	1.66	1.5	1.66	1.42	1.39	1.59	1.47	1.44	1.41
Cr	0	0	0	0	0	0	0	0	0	0	0	0
Fe	0	0	0	0	0	0	0	0	0	0	0	0
Mn	0	0	0	0	0	0	0	0	0	0	0	0
Mg	0	0.01	0.01	0.01	0	0	0	0.07	0.01	0	0	0
Ca	0.88	0.65	0.84	0.69	0.49	0.69	0.42	0.41	0.61	0.46	0.42	0.4
Na	0.13	0.34	0.15	0.31	0.47	0.32	0.54	0.51	0.37	0.5	0.54	0.55
K	0	0.01	0	0.01	0.03	0.01	0.04	0.04	0.02	0.04	0.04	0.05
Total	5.01	5.01	5	5.02	5.01	5.02	5.01	5.04	5.01	5.01	5.01	5.01
Ab (%)	13.25	33.7	14.97	30.71	47.35	31.62	54.15	53.12	36.68	50.2	53.65	55.56
An (%)	86.58	64.91	84.62	68.35	49.71	67.42	41.7	42.77	61.04	46.28	42.11	39.86
Or (%)	0.16	1.38	0.41	0.95	2.94	0.96	4.15	4.11	2.28	3.52	4.24	4.58

5.2. Basaltic trachy-andesite

Basaltic trachy-andesites are porphyritic, aphyric and less often amygdaloidal that contain pyroxene, plagioclase and minor amphibole (Fig. 3d,e). In some samples, the grain size of plagioclase reaches up to 3 cm (Fig. 3f). Matrix contains plagioclase and pyroxene, the accessory minerals are opaque, alkali feldspar and apatite. Biotite is observed in some samples which can be the alteration product of mafic minerals.

6. Mineral chemistry

6.1. Olivine

Representative compositions of olivines in south Marzanabad volcanic rocks, are displayed in Table 1. The olivine cores of alkali-olivine basalts have higher MgO and lower FeO, CaO and MnO rather than rims (Fig. 4). Their cores and rims reveal $Fo_{71\text{-}86}$ and $Fo_{67\text{-}81}$ composition respectively.

Table 4
Representative microprobe analysis of amphiboles in south Marzanabad volcanic rocks (oxides are in wt.% and elements are in apfu). Calculation is based on 22 oxygen.

Sample	CA24	CA24	CA24	CA24	CA24	CA24	CA24	CA24	CA24	CA2	CA24	CA24
Na_2O	2.54	2.55	2.53	2.52	2.54	2.58	2.54	2.16	2.1	2.56	1.39	2.57
MgO	11.68	11.61	11.64	11.62	11.76	11.3	11.85	11.76	11.21	11.35	11.73	11.76
Al_2O_3	13.6	13.74	13.88	13.86	13.32	13.78	13.29	13.51	14.07	14.02	13.78	13.9
SiO_2	39.4	39.06	38.83	38.98	41.06	39.15	41.18	38.95	39.79	38.95	38.64	39.01
K_2O	1.13	1.1	1.09	1.08	1.09	1.1	1.01	1.01	1.04	1.06	1.05	1.06
CaO	10.55	10.45	10.48	10.53	10.22	10.5	10.82	10.73	10.15	10.08	10.59	10.52
TiO_2	6.68	6.62	6.74	6.73	6.54	6.64	6.32	6.27	6.03	6.8	6.96	6.9
Cr_2O_3	0.02	0.03	0	0	0.02	0.03	0.02	0	0	0	0	0.03
MnO	0.18	0.16	0.13	0.13	0.17	0.17	0.17	0.19	0.16	0.15	0.19	0.11
FeO	12.18	12.81	12.4	12.69	12.37	12.98	11.96	12.14	12.16	12.57	12.12	12.36
Total	97.95	98.13	97.73	98.13	99.09	98.22	99.16	96.72	96.7	97.55	96.45	98.21
Si	5.81	5.75	5.73	5.73	5.95	5.77	5.99	5.79	5.88	5.74	5.71	5.73
Al^{IV}	2.19	2.25	2.27	2.27	2.05	2.23	2.01	2.21	2.12	2.26	2.29	2.27
Al^{VI}	0.17	0.13	0.14	0.13	0.23	0.16	0.27	0.16	0.34	0.18	0.12	0.13
Ti	0.74	0.73	0.75	0.74	0.71	0.74	0.69	0.7	0.67	0.75	0.77	0.76
Cr	0	0	0	0	0	0	0	0	0	0	0	0
Fe^{3+}	0.27	0.43	0.39	0.41	0.3	0.34	0.09	0.42	0.43	0.45	0.67	0.37
Fe^{2+}	1.23	1.14	1.14	1.15	1.2	1.26	1.37	1.09	1.08	1.1	0.83	1.15
Mn	0.02	0.02	0.02	0.02	0.02	0.02	0.02	0.02	0.02	0.02	0.02	0.01
Mg	2.57	2.55	2.56	2.55	2.54	2.48	2.57	2.61	2.47	2.5	2.59	2.57
Ca	1.67	1.65	1.66	1.66	1.59	1.66	1.69	1.71	1.61	1.59	1.68	1.66
Na	0.73	0.73	0.72	0.72	0.71	0.74	0.71	0.62	0.6	0.73	0.4	0.73
K	0.21	0.21	0.21	0.2	0.2	0.21	0.19	0.19	0.2	0.2	0.2	0.2
Total	15.39	15.37	15.38	15.38	15.3	15.39	15.4	15.33	15.21	15.32	15.08	15.39
$Mg^{\#}$	0.68	0.69	0.69	0.69	0.68	0.66	0.65	0.7	0.7	0.69	0.76	0.69

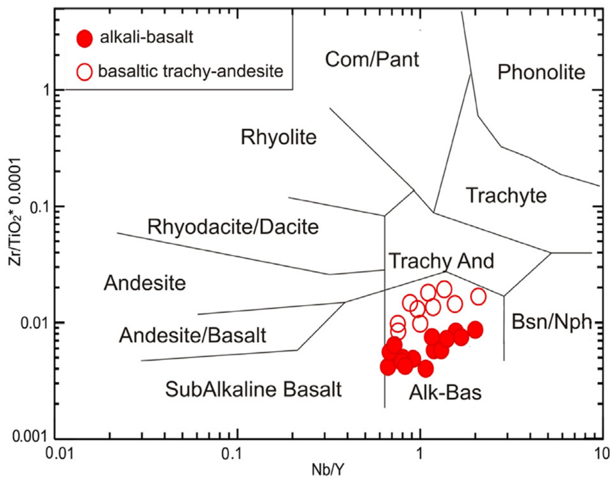

Figure 6. Classification of south Marzanabad volcanic rocks according to Winchester and Floyd (1977).

6.2. Clinopyroxene

Representative compositions of pyroxenes are shown in Table 2. Pyroxene is the main mineral in both alkali-basalts and basaltic trachy-andesites. Their cores are enriched of Mg, Si and Cr, and depleted of Fe, Ti, Al, Ca and Mn.

According to pyroxene classification diagram (Morimoto et al., 1988), all analyzed samples are located in diopside field (Fig. 5a,b). Composition of pyroxenes in alkali-basalts and basaltic trachy-andesites ranges from $Wo_{47.9}Fs_{4.5}En_{47.6}$ to $Wo_{49.8}Fs_{12.6}En_{37.6}$ and from $Wo_{44.8}Fs_{10.7}En_{44.5}$ to $Wo_{49.5}Fs_{13.6}En_{36.9}$ respectively. Both TiO_2 and Al_2O_3 show the greatest variation among oxides. TiO_2 ranges from 0.7 to 2.94 wt.% in alkali-basalts and from 1.53 to 3.44 wt.% in basaltic trachy-andesites. Al_2O_3 varies from 2.89 to 9.47 wt.% in alkali-basalts and from 2.25 to 6.91 wt.% in basaltic trachy-andesites. The composition of pyroxenes in groundmass is almost similar to the composition of pyroxene phenocrysts rims, but shows rather higher values of SiO_2 and FeO.

Table 5
Representative analysis of south Marzanabad volcanic rocks (oxides are in wt.% and elements are in ppm).

Sample	CA21	CA18	RD14	RD114	CA23	RD109	RD150	RD107	RD57	RD101	RD111	RD113	RD104
SiO_2	48.08	42.91	47.75	42.45	46.53	45.92	45.27	53.37	51.18	44.54	46.42	46.42	46.9
TiO_2	1.74	2.98	2	3.25	2.14	2.25	2.05	1.56	1.98	3.19	2.39	2.39	2.4
Al_2O_3	18.86	14.1	14.83	15.22	17.29	17.37	15.83	18.16	17.51	15.11	17.92	17.92	17.86
Fe_2O_3	12.1	17.4	12.12	17.16	12.64	12.89	12.89	9.24	9.6	16.35	13.39	13.39	13.48
MnO	0.13	0.3	0.15	0.18	0.2	0.22	0.19	0.16	0.23	0.16	0.2	0.2	0.22
MgO	5.11	7.26	10.31	7.33	7.92	7.07	11.68	2.92	4.45	7.18	4.6	4.6	5.1
CaO	10.61	10.67	9.32	9.82	10.42	10.42	8.92	8.84	8.56	9.79	10.98	10.98	8.99
Na_2O	2.33	1.57	2.08	2.14	2.29	3.3	1.75	4.85	5.4	2.19	3.13	3.13	3.94
K_2O	0.74	1.18	0.97	0.83	0.29	0.25	1.03	1.26	0.52	0.82	0.59	0.59	0.73
P_2O_5	0.31	0.64	0.47	0.63	0.29	0.31	0.39	0.64	0.57	0.67	0.37	0.37	0.38
Sum	100	99	100	99	100	100	100	101	100	100	100	100	100
L.O.I	2.3	1.9	2.3	3.5	2.3	2.1	3	0.7	1.2	2.1	1.4	1.8	2
Ba	236	440	292	428	188	201	280	455	349	374	322	288	230
Co	46	60	51	58	53	60	57	47	33	55	47	41	44
Cr	41	200	222	161	136	153	218	6	3	152	44	48	47
Cu	62	52	22	54	56	25	99	8	29	56	26	19	25
Ga	18	21	16	23	15	17	18	18	17	21	21	20	19
Hf	3	7	5	6	3	5	4	4	5	8	5	5	5
Nb	13	21	36	38	18	20	29	50	41	43	22	22	19
Nd	19	38	27	46	19	17	20	34	37	48	28	30	25
Ni	10	170	99	103	37	35	94	0	0	100	9	10	10
Rb	4	10	4	0	0	0	3	11	2	0	3	0	6
Sc	34	25	24	21	30	30	24	8	13	23	35	36	38
Sr	350	656	652	765	562	677	531	663	737	788	479	486	672
Th	4	6	4	6	5	5	4	4	6	7	5	5	6
V	355	316	213	261	306	341	238	109	150	258	401	393	377
Y	21	23	23	32	23	25	25	24	35	34	35	34	31
Zn	99	99	70	108	75	77	85	99	105	94	92	97	102
Zr	81	143	165	186	99	110	153	402	358	368	153	149	130
La		29.1			25.5								
Ce		66			29								
Pr		7.93			3.76								
Sm		6.57			3.92								
Eu		2.01			1.39								
Gd		5.72			3.68								
Tb		0.88			0.64								
Dy		3.86			3.1								
Ho		0.7			0.61								
Er		1.69			1.55								
Tm		0.23			0.23								
Yb		1.26			1.29								
Lu		0.17			0.18								
Hf		4.29			1.88								
Ta		1.83			1.01								
U		0.87			0.47								

Sample	RD142	RD29	CA53	RD7	CA20	RD125	RD26	RD140	RD127	RD56	RD57	CA52	RD100
SiO_2	43.82	46.93	43.86	44.28	52.18	54.08	48.36	49.89	44.97	49.49	51.18	51.8	44.01
TiO_2	2.88	2.26	3.26	2.11	1.6	1.49	2.2	1.79	2.97	2.05	1.98	2.66	3.19

(continued on next page)

Table 5 (*continued*)

Sample	RD142	RD29	CA53	RD7	CA20	RD125	RD26	RD140	RD127	RD56	RD57	CA52	RD100
Al_2O_3	16	16.94	13.37	15.72	18.18	18.09	18.05	17.68	14.52	18.1	17.51	16.88	15.07
Fe_2O_3	15.28	12.93	14.27	12.83	10.15	9.05	12.21	11.29	15.9	11.21	9.6	10.52	16.83
MnO	0.18	0.2	0.17	0.17	0.18	0.16	0.17	0.17	0.18	0.28	0.23	0.14	0.16
MgO	9.62	5.82	10.77	11.83	3.27	3.24	3.48	5.18	8.08	3.64	4.45	4.59	6.96
CaO	7.95	11.42	10.01	9.68	8.41	6.34	11.05	8.91	8.63	8.83	8.56	7.76	10.02
Na_2O	1.77	2.91	3.18	1.73	3.97	5.76	3.26	3.33	1.85	5.47	5.4	3.28	2.21
K_2O	1.74	0.27	0.46	1.23	1.35	1.24	0.92	1.01	2.11	0.47	0.52	1.61	0.89
P_2O_5	0.75	0.3	0.66	0.41	0.71	0.55	0.29	0.73	0.78	0.57	0.57	0.77	0.67
Sum	100	100	100	100	100	100	100	100	100	100.1	100	100	100
L.O.I	2.4	1.5	2.4	2.4	0.6	1.6	1.3	1.6	2.1	2.3	1.2	3.3	1.8
Ba	376	208	782	324	518	461	375	514	559	296	350	821	352
Co	49	54	67	59	21	28	41	33	52	47	33	50	51
Cr	12	142	453	248	0	12	46	1	149	25	3	41	153
Cu	59	34	77	92	3	12	42	15	51	20	29	42	55
Ga	19	16	17	18	18	18	19	19	23	20	17	21	22
Hf	6	4	6	3	4	6	4	4	8	5	5	7	7
Nb	56	19	61	35	28	29	19	24	24	31	41	40	42
Nd	40	19	33	19	39	33	19	40	54	28	37	64	54
Ni	37	36	197	117	0	2	10	0	86	6	0	22	103
Rb	8	1	2	5	16	13	12	3	18	0	2	33	0
Sc	17	37	31	27	10	8	31	13	18	18	13	14	25
Sr	886	392	573	325	608	1023	303	718	1235	1006	738	823	792
Th	6	5	8	4	3	5	5	3	7	4	6	9	6
V	193	327	307	242	88	150	357	137	239	261	150	199	253
Y	28	24	32	25	27	30	31	27	29	24	35	34	34
Zn	81	71	82	80	81	82	85	99	103	92	105	74	96
Zr	248	104	290	151	255	194	132	156	124	155	358	359	366
La		13.7	40.1	23.8	13.7	47.6	21.2	34.4					40.5
Ce		78	29	44	78	93	41	69					82
Pr		8.97	3.82	4.8	10.37	11.18	5.54	8.96					10.15
Sm		6.58	3.89	4	9.68	8.3	5.38	7.6					8.1
Eu		2.04	1.38	1.33	3.1	2.59	1.67	2.68					2.54
Gd		5.81	3.64	3.87	8.16	7.18	5.07	6.92					7.19
Tb		0.86	0.63	0.64	1.24	1.08	0.89	1.12					1.13
Dy		3.74	3.02	3.02	5.01	4.67	4.39	5.17					5.09
Ho		0.68	0.59	0.58	0.83	0.84	0.9	1.01					0.94
Er		1.69	1.51	1.45	1.84	2.05	2.41	2.6					2.36
Tm		0.24	0.22	0.21	0.23	0.28	0.38	0.39					0.33
Yb		1.3	1.22	1.15	1.17	1.55	2.22	2.22					1.84
Lu		0.18	0.17	0.16	0.15	0.21	0.32	0.32					0.26
Hf		4.54	1.69	2.16	2.31	5.14	2.48	2.65					3.89
Ta		3.27	0.97	1.56	2.48	2.85	1.04	1.47					2.2
U		1.51	0.48	0.68	1.27	1.35	1.05	0.92					0.9

6.3. *Plagioclase*

Representative compositions of plagioclases are listed in Table 3. In Ab-An-Or ternary diagram, they present wide range of composition from andesine to bytownite (Fig. 5c,d). Na_2O and K_2O increase from core toward rim, whereas CaO decreases. The composition of plagioclases in alkali-basalts varies from $Ab_{13.2}$-$An_{86.59}Or_{0.16}$ at core to $Ab_{47.35}An_{49.71}Or_{2.93}$ at rim and in basaltic trachy-andesites ranges from $Ab_{36.67}An_{61.04}Or_{2.27}$ at core to $Ab_{55.56}An_{39.86}Or_{4.57}$ at rim.

6.4. *Amphibole*

Representative compositions of amphiboles are presented in Table 4. Amphiboles of basaltic trachy-andesite samples, plot in the fields of pargasite and ferroan pargasite. They represent the kaersutite composition due to high Ti content [Ti (apfu) > 0.5] (Leake et al., 1997) (Fig. 5e,f). No systematic variation or zoning pattern observed in Kaersutite phenocrysts.

7. Whole rock chemistry

7.1. *Major element geochemistry*

South Marzanabad volcanic rocks are compositionally alkali-basalts and basaltic trachy-andesite according to Winchester and Floyd (1977) classification diagram (Fig. 6).

SiO_2, MgO and $Mg^{\#}$ [$Mg^{\#} = 100 \times Mg/(Mg + Fe^{T})$] ranges from 43.45 to 52.36 wt.%, 2.92 to 11.81 wt.% and 36 to 64.63, respectively (Table 5). According to Frey et al. (1978) primitive magmas have $Mg^{\#} > 68$ and Ni > 320 ppm. The most nearer sample to primitive composition has $Mg^{\#} = 64.63$ and Ni $= 117$ ppm. The low Ni content in this sample could signify the fractionation of olivine and Cpx (Wörner, 1999).

Basaltic trachy-andesites have higher SiO_2, Al_2O_3 and $Na_2O + K_2O$ with lower MgO content compared to alkali-basalts (Fig. 7a–c). In CaO versus MgO and SiO_2 versus Al_2O_3 diagrams, both decreasing and increasing trends are observed (Fig. 7d,h). MgO versus CaO/Na_2O diagram, shows positive trend in south Marzanabad volcanic rocks (Fig. 7f).

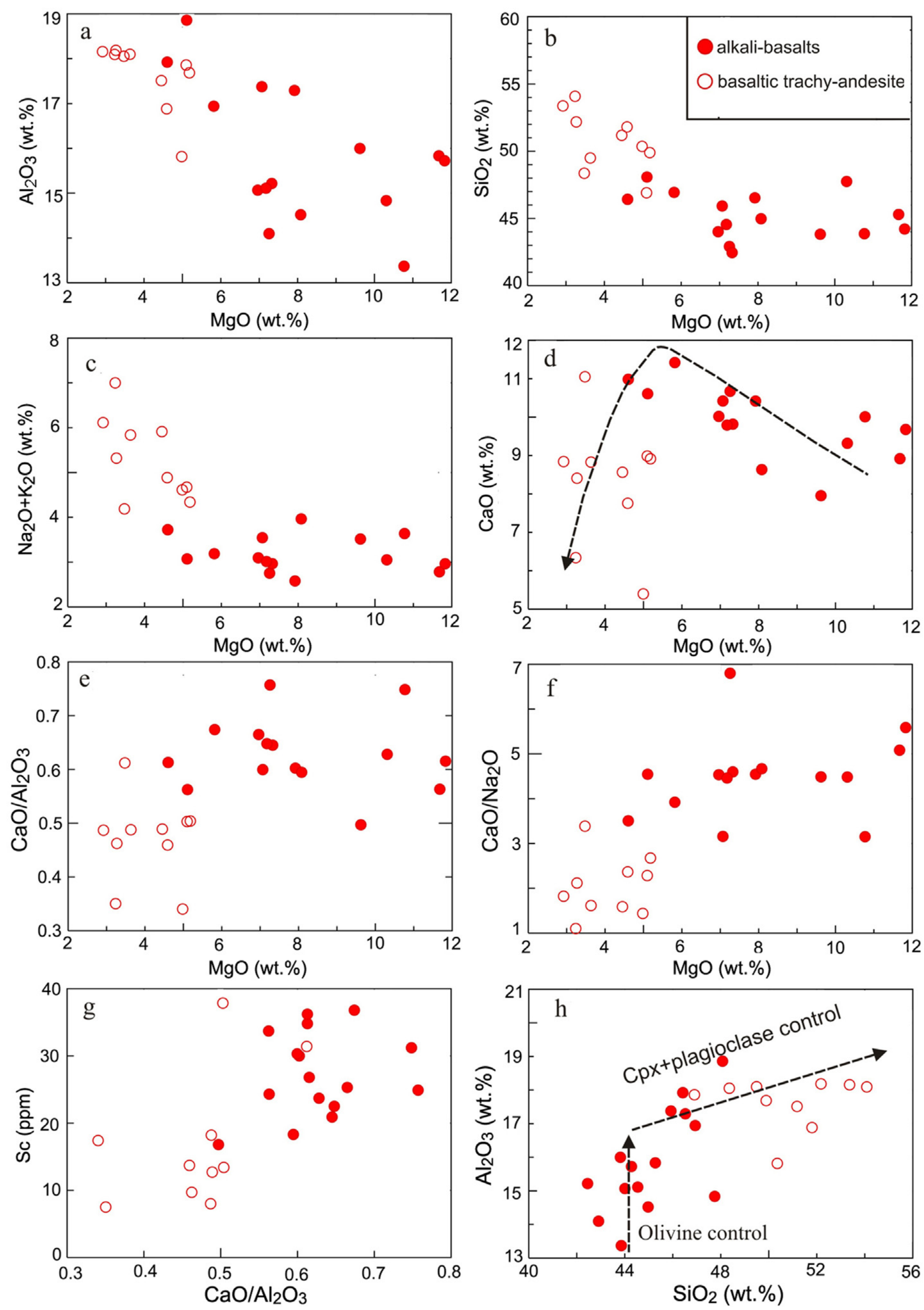

Figure 7. (a) MgO versus Al_2O_3, (b) MgO versus SiO_2, (c) MgO versus $Na_2O + K_2O$, (d) MgO versus CaO, (e) MgO versus CaO/Al_2O_3, (f) MgO versus CaO/Na_2O, (g) CaO/Al_2O_3 versus Sc, (h) SiO_2 versus Al_2O_3 in south Marzanabad volcanic rocks.

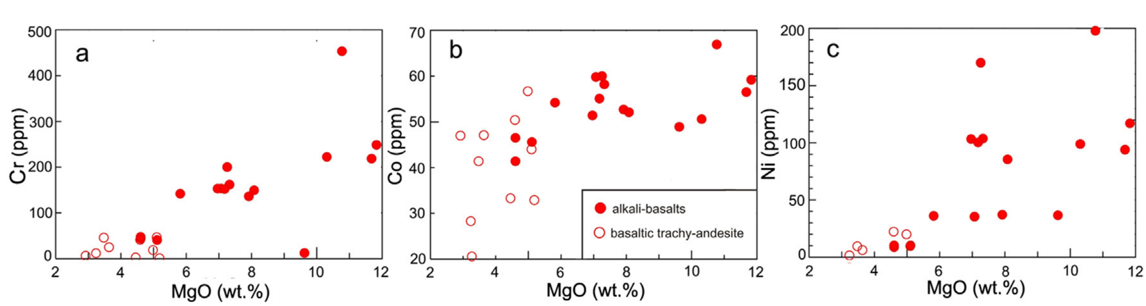

Figure 8. (a) MgO versus Cr, (b) MgO versus Co, (c) MgO versus Ni in south Marzanabad volcanic rocks.

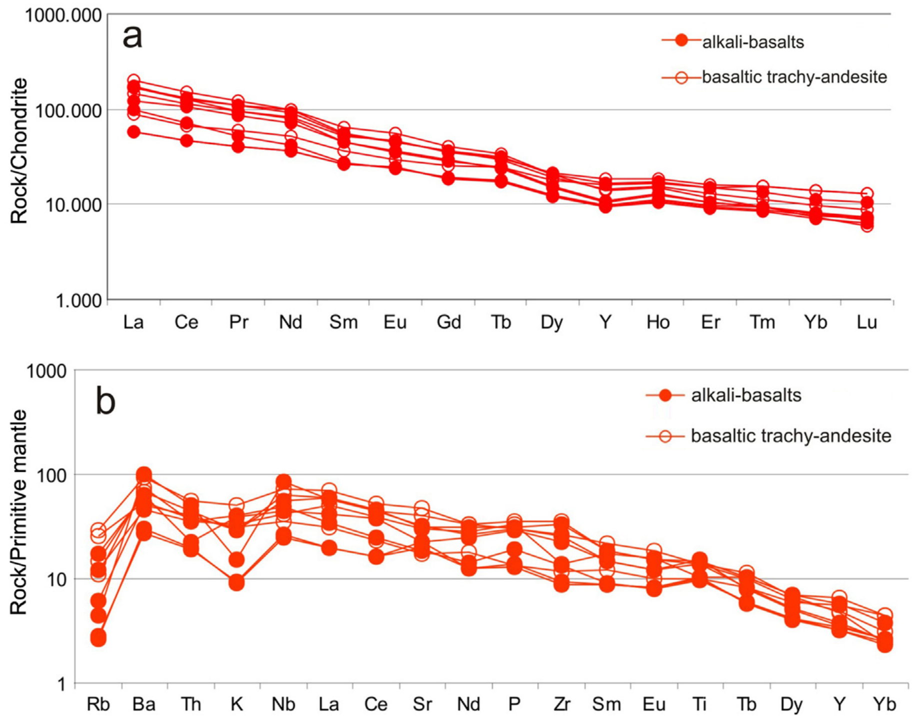

Figure 9. (a) Chondrite normalized diagram for south Marzanabad volcanic rocks, normalized values are from McDonough and Sun (1995). (b) Primitive mantle normalized diagram for south Marzanabad volcanic rocks, normalized values are from McDonough and Sun (1995).

7.2. Trace element and isotopic geochemistry

Ni, Co and Cr represent positive correlation with increasing MgO in both groups of alkali-basalts and basaltic trachy-andesites (Fig. 8). They respectively vary from 453 to 12 ppm, from 198 to 9 ppm and from 67 to 46 ppm in alkali-basalts and from 47 to 0 ppm, from 22 to 0 ppm and from 47 to 21 ppm in basaltic trachy-andesites.

South Marzanabad volcanic rocks are enriched in LREE respect to HREE and show the similar trend with OIB basalts and continental alkaline volcanic rocks (Beccaluva et al., 2002; Bianchini et al., 2002; Beccaluva et al., 2009) (Fig. 9a). They show enrichment of Nb and depletion of Rb, K and Y (Fig. 9b).

The $(La/Yb)_N$ ratio in both groups of rocks almost is similar and ranges from 7.00 to 20.93 with an average of 13.53. The $(Dy/Yb)_N$ ratio almost is similar in all samples and varies from 1.30 to 2.80 with an average of 1.81. Small positive Eu anomalies ($Eu/Eu^* = 1.00–1.12$) are displayed in all samples, except one basaltic trachy-andesite sample, that shows small Eu negative anomaly (0.97).

Isotopic analyses of south Marzanabad volcanic rocks are represented in Table 6. Studied samples locate in the depleted part relative to bulk earth composition regard to their low $^{87}Sr/^{86}Sr$ (0.70370–0.704387) and high $^{143}Nd/^{144}Nd$ (0.51266–0.51281) (Fig. 10). They represent the isotopic composition of OIB field. More evolved sample from basaltic trachy-andesite group with low $Mg^{\#}$ has more radiogenic $^{87}Sr/^{86}Sr$ and less radiogenic $^{143}Nd/^{144}Nd$.

8. Discussion

8.1. Fractional crystallization

Based on petrographical studies (Section 4), south Marzanabad volcanic rocks reveal the evolutionary trend.

For both alkali-basalts and basaltic trachy-andesites, negative correlations between SiO_2, Al_2O_3 and $Na_2O + K_2O$ with increasing MgO, can indicate the derivation of volcanic rocks from the same parental magma, during fractional crystallization (Fig. 7a–c). In CaO versus MgO diagram, negative trend for MgO values more than 7 wt.%, implies the fractionation of olivine and remaining CaO in magma, whereas the fractionation of Cpx and plagioclase assumes CaO and causes positive trend for MgO values less than 7 wt.% (Rollinson, 1998) (Fig. 7d).

The correlation trend between MgO and CaO/Na_2O can reveal Cpx fractionation (Herzberg and Zhang, 1996; Machado et al., 2005) (Fig. 7f). SiO_2 versus Al_2O_3 diagram (Fig. 7h) displays olivine

Table 6
Rb, Sr, Nd and Sm concentrations and present-day Nd and Sr isotopic ratios for south Marzanabad volcanic rocks.

Sample	$^{87}Sr/^{86}Sr$	2σ	Rb (ppm)	Sr (ppm)	Rb/Sr	$^{87}Rb/^{86}Sr$	$^{143}Nd/^{144}Nd$	2σ	Sm (ppm)	Nd (ppm)	Sm/Nd	$^{147}Sm/^{144}Nd$
RD29	0.703703	0.0033	1.14	392.12	0.0029	0.0084	0.51275	0.0044856	3.89	16.9	0.23	0.14
CA53	0.704075	0.0037	1.91	573.12	0.0033	0.0096	0.512811	0.00507	6.6	32.9	0.2	0.12
RD7	0.703786	0.004	5.22	325.34	0.016	0.0464	0.51275	0.0050707	4.00	19.3	0.21	0.13
RD26	0.704387	0.0037	11.16	303.39	0.0368	0.1064	0.512666	0.0050715	5.38	24	0.22	0.14

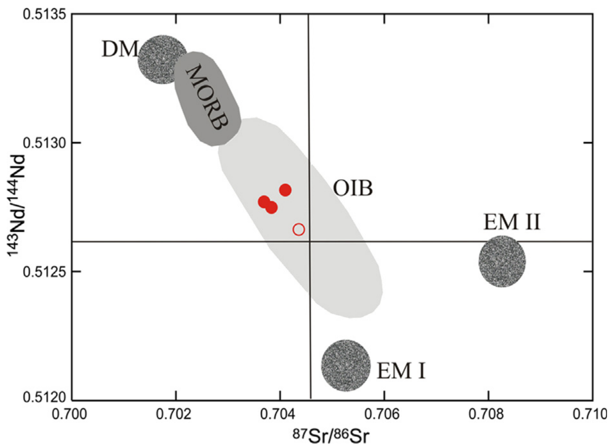

Figure 10. Sr-Nd isotopic diagram for south Marzanabad volcanic rocks. The two types enriched mantle (EMI and EMII), depleted MORB mantle (DM) and OIB field are also shown in this diagram.

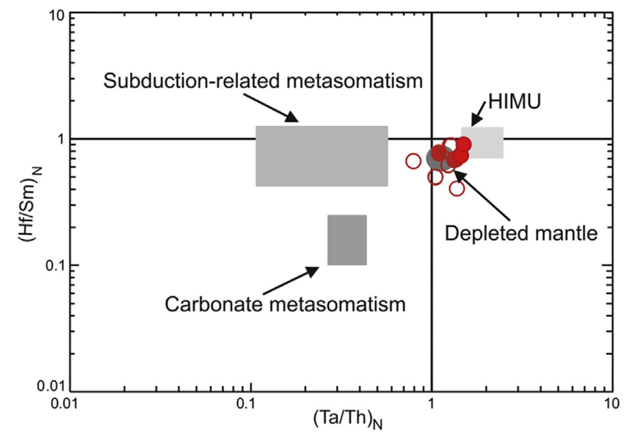

Figure 12. South Marzanabad volcanic rocks on the diagram of $(Ta/Th)_N$ and $(Hf/Sm)_N$ from Wang et al. (2006). All samples locate in the field of depleted mantle.

fractionation in alkali-basalts and Cpx or plagioclase fractionation in the basaltic trachy-andesites (Wilson, 1989).

Basaltic trachy-andesites show the lowest Ni, Cr and V, which indicate olivine and Cpx were important fractionating mineral phases in the petrogenesis of south Marzanabad volcanic magmas. Basaltic trachy-andesites reveal higher Ba/Nb, K/Nb, Zr/Nb and Rb/Nb than alkali-basalts that display the effect of fractionation process in their evolution. The average values of Ba/Nb, K/Nb, Zr/Nb and Rb/Nb ratios in alkali-basalts and basaltic trachy-andesites are 12.79, 273, 6, 0.14 and 15.31, 316, 8, 0.36 respectively.

Decreasing Al_2O_3 with increasing MgO and small Eu anomalies indicate that plagioclase was not a major fractionating mineral phase during the evolution of the magma, pointing that the fractionation of studied rocks could occur in depth >15 km which is correlated with pressures >5 kbar in lower crust (Jung et al., 2006).

The MELTS software is used for reconstructing the fractional crystallization process in south Marzanabad volcanic rocks. MELTS is based on the work of Ghiorso and Sack (1995) and Asimow and Ghiorso (1998). In present model, the sample RD7 was assumed as a source magma that is the most primitive and undifferentiated alkali-basalt with the highest Ni and Cr. Based on this model the major element composition of alkali-basalts could be explained by almost 30% of fractional crystallization, whereas basaltic trachy-andesites could be explained by up to almost 50% of fractional crystallization (Fig. 11).

8.2. Crustal contamination and source magma

The K/Nb ratio in the studied samples varies from 62 to 588 and is averagely higher in evolved samples. This ratio ranges from 62 to 588 in alkali-basalts with an average of 234 and from 100 to 540 in basaltic trachy-andesites with an average of 316. Based on Taylor

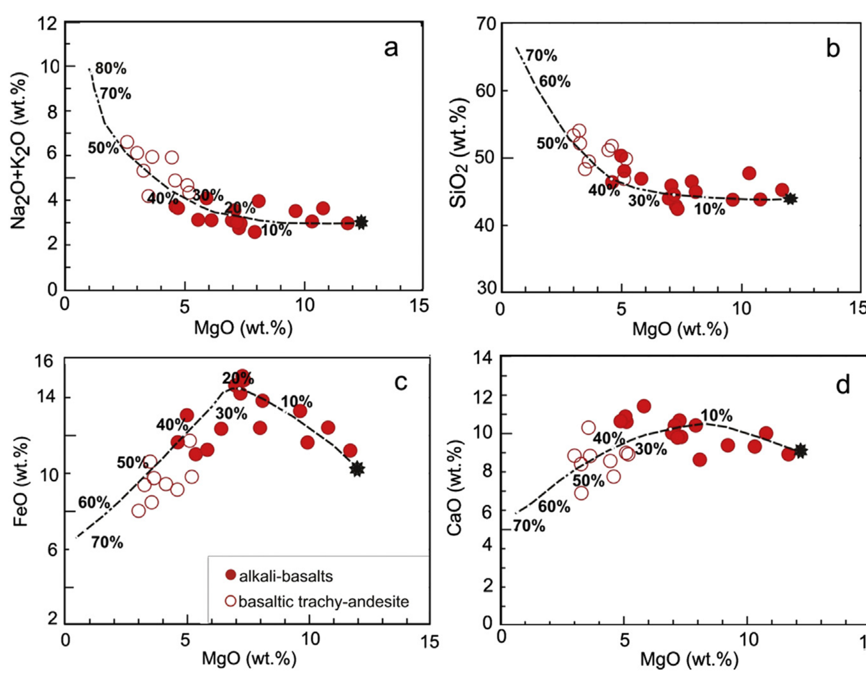

Figure 11. (a) MgO versus $Na_2O + K_2O$, (b) MgO versus SiO_2, (c) MgO versus FeO, (d) MgO versus CaO in south Marzanabad volcanic rocks. Lines represent the results of fractional crystallization calculation by MELTS software with numbers that indicate the mass crystallized as wt.%.

and McLennan (1985) K/Nb in the Earth's crust is higher than mantle. More values of K/Nb in basaltic trachy-andesites could show the occurrence of some minor crustal contamination (Jung et al., 2006).

In primitive mantle normalized diagram, basaltic trachy-andesites show less depletion of K compared to alkali-basalts which may reflect the effect of minor crustal contamination or fractional crystallization. Zr/Nb varies from 4.27 to 5.59 in alkali-basalts which are less evolved; however in more evolved basaltic trachy-andesites, Zr/Nb ranges from 6.43 to 9, which could remark the effect of minor crustal contamination (Wörner, 1999).

The HFSE/LREE ratio can indicate the characters of source magma. According to Smith et al. (1999) ratios more than unity represent the asthenospheric origin for magma, whereas ratios less than unity represent the lithospheric origin. In south Marzanabad volcanic rocks Nb/La, Zr/La and Zr/Ce ratios are 1.15, 4.51 and 2.23 respectively, which suggest the melt origination from an asthenospheric mantle. Based on rare earth elements and isotopic composition, the studied rocks show the similar source characteristics and derive from the same magmatic source in depleted mantle with regard to bulk earth composition (Fig. 12).

8.3. Crystallization condition

Low Ti/Al ratios in Cpx composition specify the crystallization of Cpx in low pressures (e.g., Wilkinson, 1974; Dobosi et al., 1991; Wlodyka, 2002; Ali and Ntaflos, 2011). The Ti/Al ratio varies from 0.077 to 0.513 in alkali-basalts and from 0.154 to 0.537 in basaltic trachy-andesites (Fig. 13a). The average of this ratio in alkali-basalts and basaltic trachy-andesites respectively is 0.20 and 0.34. Concerning the lower Ti/Al ratio in Cpx of alkali-basalts, they could be crystallized in rather higher pressures than Cpx of basaltic trachy-andesites. On the other hand, increasing of Al^{VI}/Al^{IV} ratio in Cpx, shows the pressure increment during crystallization (Green and Ringwood, 1968; Wass, 1979). Al^{VI}/Al^{IV} ratio varies from 0.00 to 0.49 in alkali-basalts with an average of 0.24 and from 0.00 to 0.39 in basaltic trachy-andesites with an average of 0.07 (Fig. 13b). As a result, the crystallization of Cpx in alkali-basalts took place in slightly higher pressures than Cpx in basaltic trachy-andesites.

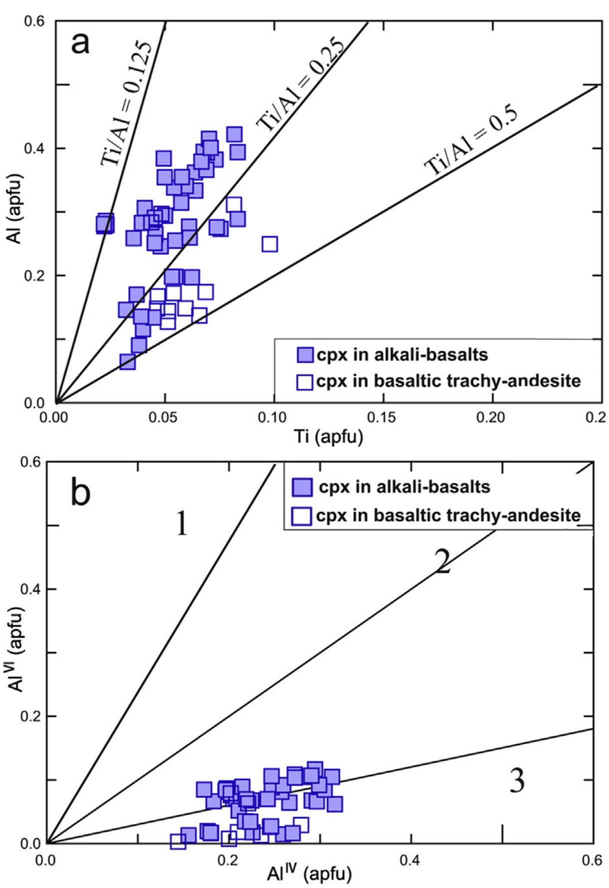

Figure 13. (a) Ti versus Al diagram in the pyroxenes of south Marzanabad volcanic rocks. (b) Plot of Al^{VI} versus Al^{IV} in the pyroxenes of south Marzanabad volcanic rocks (calculation is based on 6 oxygens), fields are: 1–eclogites, 2–granulites and inclusions in basalts, 3–igneous rocks (Aoki and Shiba, 1973).

8.4. Partial melting of source magma and mantle potential temperature

The differentiation degree of LREE relative to HREE is defined by the $(La/Yb)_N$ ratio that varies from 7.00 to 20.93 with an average of 13.53 in south Marzanabad volcanic rocks. High $(La/Yb)_N$ in studied rocks suggests the low degree of partial melting in their mantle source (Jung et al., 2006).

The HREE enrichment degree is represented by the $(Dy/Yb)_N$ ratio. The partial melts generated from garnet-lherzolite source, have $(Dy/Yb)_N > 1.06$ (Blundy et al., 1998; Peters et al., 2008). $(Dy/Yb)_N$ ratio ranges from 1.29 to 2.80 with an average of 1.81 in Marzanabad volcanic rocks, which signifies the garnet was a residual phase during the partial melting.

We used PRIMELT2.XLS software from Herzberg and Asimow (2008) to calculate primary magma composition and mantle potential temperature. The four most primitive rock samples of south Marzanabad volcanic rocks plot above the dashed-line in Fig. 14 that characterizes olivine-fractionated primary magma from peridotitic sources. For calculating the most proper primary magma composition for Marzanabad volcanic rocks, we used the most primitive RD7 sample with $Fe_2O_3/TiO_2 = 1.0$ to estimate Fe_2O_3 (Herzberg and Asimow, 2008). The calculated primary magma composition have 44.75 SiO_2, 2.13 TiO_2, 15.89 Al_2O_3, 2.13 Fe_2O_3, 9.75 FeO, 11.95 MgO and 9.78 CaO (all in wt.%).

The calculated mantle potential temperature for Marzanabad volcanic rocks is 1370 °C. The ambient mantle potential temperatures that make MORB is about 1300–1454 °C (Herzberg et al., 2007; Putirka et al., 2007), showing that the Marzanabad volcanic rocks come up from an ambient mantle.

For modeling the partial melting of common upper mantle source, REE systematics like the plot of La/Yb vs. Dy/Yb (Fig. 15) can

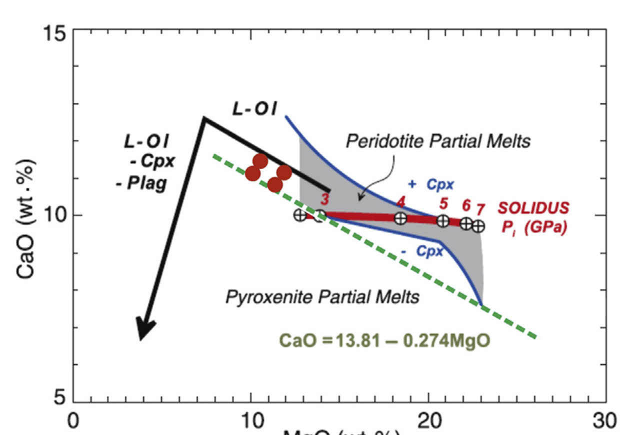

Figure 14. CaO and MgO diagram of the south Marzanabad volcanic rocks compared with partial melts of pyroxenite and peridotite (Herzberg and Asimow, 2008).

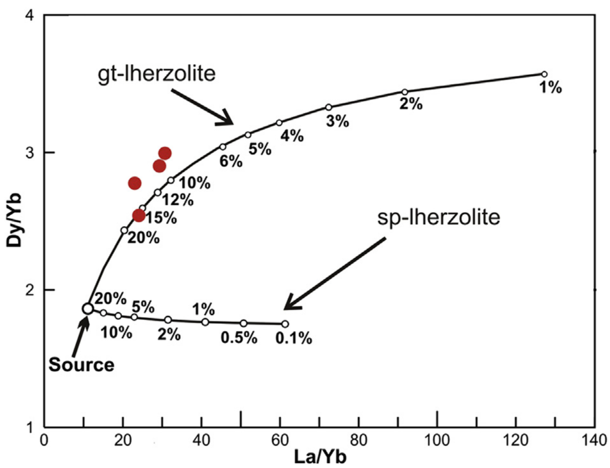

Figure 15. La/Yb vs. Dy/Yb covariation for the south Marzanabad volcanic rocks. Partial melting curves were calculated using a non-modal, fractional melting model (Shaw, 1970).

be useful (Thirlwall et al., 1994; Baker et al., 1997; Jung et al., 2006). This plot is easily recognizes between melting in the garnet peridotite stability field and spinel peridotite stability field owing to the strong fractionation of HREE by garnet.

Partial melting in the source magma of south Marzanabad volcanic rocks was reconstructed (Fig. 15). Partial melting curves were calculated using a modal, fractionated melting model (Shaw, 1970). Mineralogical composition of primitive mantle (66% olivine, 14% orthopyroxene, 14% clinopyroxene, 6% garnet) and chemical composition of primitive mantle are taken from Mertz et al. (2001). Mineral-melt distribution coefficients are taken from McKenzie and O'Nions (1991, 1995) and normalizing values are from McDonough and Sun (1995). In both diagrams of Figs. 15 and 16, the most primitive RD7 sample, reveals nearly 15% of partial melting in the garnet peridotite stability field, which produces the primary magma of south Marzanabad volcanic rocks.

8.5. Melt generation

The alkali basalt magmatism in central Alborz is related to deep mantle melting or mantle plume associated with crustal contamination in local extensional system or deep faults system (Haghnazar et al., 2009; Jaffarian et al., 2009). Alborz zone reveals

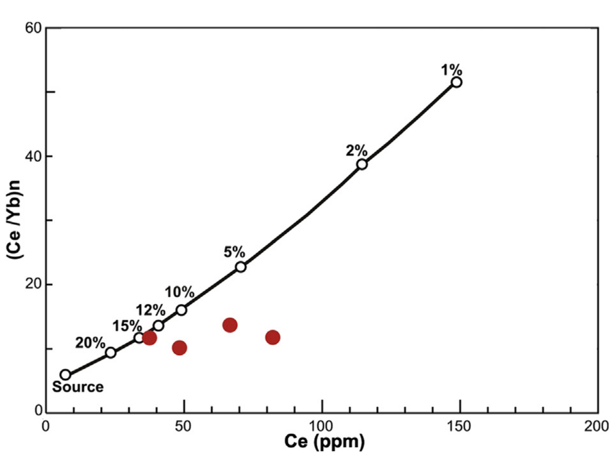

Figure 16. Chondrite normalized Ce/Yb vs. Ce for south Marzanabad volcanic rocks. Normalization values are from McDonough and Sun (1995).

an elevation 3000–5000 m above sea level. According to geophysical studies, mantle lithosphere is almost absent underneath the Alborz Mountains (e.g., Sodoudi et al., 2009; Mirnejad et al., 2010). The crustal thickness under the central Alborz is estimated about 35–45 km (Dehghani and Makris, 1984; Amjadi et al., 2012). However insufficient crustal base and the relatively thin lithosphere underneath the Alborz can predicate that the asthenospheric mantle is backing the high elevation (Sodoudi et al., 2009). Ansari et al. (2011) believed that alkaline magmatism in central Alborz zone was generated by the deep mantle melting and the delamination of sub-continental lithosphere.

The calculated mantle potential temperature shows that south Marzanabad volcanic rocks generated from the mantle at ambient temperature which is against the mantle plume hypothesis (Hastie and Kerr, 2010).

In summary, in south Marzanabad area in north of central Alborz, like many other parts of Iran, an extensional rift basin was originated during Cretaceous. Based on isotopic and REE data of south Marzanabad volcanic rocks, alkaline volcanism was occurred by the extension and partial melting of asthenospheric mantle in the rift basin without major affecting of contribution subcontinental lithospheric mantle or crustal contamination. Erupted alkaline volcanic rocks overlapped the upper Jurassic Shemshak sediments with the angular unconformity. Existence of magmatic chambers en route of ascending magma could cause crystal fractionation. Finally in late Cretaceous, the Laramide orogenic phase terminated the rifting extensional system and volcanism.

9. Conclusion

South Marzanabad volcanic rocks underwent fractional crystallization that is confirmed by petrographical and geochemical studies. Basaltic trachy-andesites formed from alkali-basalts due to fractional crystallization. Based on the presented fractionation model of south Marzanabad volcanic rocks, the composition of more evolved samples could be explained by up to almost 50% of fractional crystallization.

The source magma of south Marzanabad rocks was generated by the low degree of partial melting from the garnet bearing mantle source with regard to high values of $(La/Yb)_N$ and $(Dy/Yb)_N$. Based on low $^{87}Sr/^{86}Sr$, high $^{143}Nd/^{144}Nd$ and HFSE/REE ratios, south Marzanabad volcanic rocks show the similar source characteristics and derivation from the depleted mantle source with regard to bulk earth composition.

The calculated mantle potential temperature shows that south Marzanabad volcanic rocks generated from the mantle at ambient temperature which is contrary to mantle plume hypothesis. In Cretaceous, alkaline volcanism was occurred by upwelling and decompressional melting of an asthenospheric mantle in the rifting basin without major involvement of subcontinental lithospheric mantle or crustal contamination.

Acknowledgments

The authors thank Dr. Luigi Beccaluva and Dr. Renzo Tassinari, University of Ferrara, Italy, for their financial support and providing laboratory facilities.

References

Alavi, M., 1991. Sedimentary and structural characteristics of the Paleo-Tethys remnants in northeastern Iran. Geological Society of America Bulletin 103, 983–992.

Ali, Sh, Ntaflos, Th, 2011. Alkali basalts from Burgenland, Austria: petrological constraints on the origin of the westernmost magmatism in the Carpathian–Pannonian region. Lithos 121, 176–188.

Amjadi, A., Moteshrei, A., Theroied, S.A.A., Ansari, M.R., 2012. Estimation of Moho depth using Bouguer anomaly gravity data. Innova Ciencia l4, 7–14.
Annells, R.N., Arthurton, R.S., Bazely, R.A., Davies, R.G., 1975. Explanatory Text of the Qazvin and Rafht Quadrangles Map. Geological Survey of Iran. Geological quadrangles no. E3–E4 (with 1: 2500000 geological map).
Ansari, M.R., Vossoughi Abedini, M., Darvish Zadeh, A., Sheikhzakariaee, S.J., Hossein mirzaee Beni, Z., 2011. Geochemical constrain on the early cretaceous, OIB-type alkaline volcanic rocks in Kojor volcanic field, Central Alborz Mountain, North of Iran. Australian Journal of Basic and Applied Sciences 10, 913–925.
Aoki, K., Shiba, I., 1973. Pyroxene from lherzolithe inclusions of Itinomegata, Japan. Lithos 6, 41–51.
Asimow, P.D., Ghiorso, M.S., 1998. Algorithmic modifications extending MELTS to calculate subsolidus phase relations. American Mineralogist 83, 1127–1131.
Baker, J.A., Menzies, M.A., Thirlwall, M.F., Macpherson, C.G., 1997. Petrogenesis of quaternary intraplate volcanism, Sana'a, Yemen: implications for plume–lithosphere interaction and polybaric melt hybridization. Journal of Petrology 38, 1359–1390.
Barrier, E., Vrielynck, B., 2008. Paleotectonic Maps of the Middle East: Tectono-sedimentary-palinspastic Maps from Late Norian to Pliocene. CGMW/CCGM, Paris.
Beccaluva, L., Coltorti, M., Di Girolamo, P., Melluso, L., Milani, L., Morra, V., Siena, F., 2002. Petrogenesis and evolution of Mt. Vulture alkaline volcanism (Southern Italy). Mineralogy and Petrology 74, 277–297.
Beccaluva, L., Bianchini, G., Natali, C., Siena, F., 2009. Continental flood basalts and mantle plumes: a case study of the northern Ethiopian Plateau. Journal of Petrology 50, 1377–1403.
Berberian, M., 1979. Earthquake faulting and bedding thrust associated with the Tabas-e-Golshan (Iran) earthquake of September 16, 1978. Bulletin of the Seismological Society of America 69, 1861–1887.
Berberian, M., 1983. The southern Caspian: a compressional depression floored by a trapped, modified oceanic crust. Canadian Journal of Earth Sciences 20, 163–183.
Berberian, M., King, G.C.P., 1981. Towards a paleogeography and tectonic evolution of Iran. Canadian Journal of Earth Sciences 18, 210–265.
Berberian, F., Muir, I.D., Pankhurst, R.J., Berberian, M., 1982. Late Cretaceous and Early Miocene Andean-type plutonic activity in northern Makran and Central Iran. Journal of Geological Society of London 139, 605–614.
Best, M.G., 1970. Kaersutite-peridotite inclusions and kindred megacrysts in basanitic lavas, Grand Canyon, Arizona. Contributions to Mineralogy and Petrology 27, 25–44.
Bianchini, G., Beccaluva, L., Siena, F., 2002. Post-collisional and intraplate Cenozoic volcanism in the rifted Apennines/Adriatic domain. Lithos 101, 125–140.
Blundy, J.D., Robinson, J.A.C., Wood, B.J., 1998. Heavy REE are compatible in clinopyroxene on the spinel lherzolite solidus. Earth and Planetary Science Letters 160, 493–504.
Brunet, M.F., Korateav, M.W., Arshov, A.V., Nikishin, A.M., 2003. The south Caspian basin: a review of its evolution from subsidence modeling. Sedimentary Geology 148, 119–156.
Cartier, E.G., 1971. Die Geologic des unteren Chalus Tals, Zentral-Alborz, Iran. Inaugural-Dissertation zur Erlangtmg der Philosophischen Doktorwiirde, vorgelegt der Philosophischen Fakultät II, der Universität Zürich (in German).
Dehghani, G., Makris, J., 1984. The gravity field and crustal structure of Iran. Neues Jahrbuch für Geologie and Palaeontologie Abhundlungen 168, 215–229.
Dobosi, G., Schultz-Güttler, R., Kurat, G., Kracher, A., 1991. Pyroxene chemistry and evolution of alkali basaltic rocks from Burgenland and Styria, Austria. Mineralogy and Petrology 43, 275–292.
Ernst, R.E., Buchan, K.L., Campbell, I.H., 2005. Frontiers in large igneous province research. Lithos 79, 271–297.
Fauvelet, F., Eftekhar Nezhad, J., 1992. Explanatory Text of the Gonbad Quadrangle Map (1/250000). Geological Survey of Iran, Tehran.
Franzini, M., Leoni, L., Saitta, M., 1975. Revisione di una metodologia analitica fluorescenza-X basata sulla correzione completa degli effetti di matrice. Rendiconti della Societa Italiana di Mineralogia e Petrologia 31, 365–378 (in Italian).
Frey, F.A., Green, D.H., Roy, S.D., 1978. Integrated models of basalt petrogenesis: a study of quartz tholeiites to olivine melilitites from south eastern Australia utilizing geochemical and experimental petrological data. Journal of Petrology 19, 463–513.
Furon, R., 1941. Géologie du plateau Iranien (Perse-Afghanistan-Beloutchistan). Mém. Museum National d'histoire Naturelle, Paris, pp. 177–414 (in French).
Ganguly, J., 2005. Adiabatic decompression and melting of mantle rocks. Geophysical Research Letters 32, L06312. http://dx.doi.org/10.1029/2005GL022363.
Ghiorso, Mark S., Sack, Richard O., 1995. Chemical mass transfer in magmatic processes IV. A revised and internally consistent thermodynamic model for the interpolation and extrapolation of liquid-solid equilibria in magmatic systems at elevated temperatures and pressures. Contributions to Mineralogy and Petrology 119, 197–212.
Green, D.H., Ringwood, A.E., 1968. The stability fields of aluminous pyroxene peridotite and garnet peridotite and their relevance in upper mantle structure. Earth and Planetary Science Letters 3, 151–160.
Guest, B., Axen, G.J., Lam, P.S., Hassanzadeh, J., 2006. Late Cenozoic shortening in the west-central Alborz Mountains, northern Iran, by combined conjugate strike-slip and thin-skinned deformation. Geosphere 2, 35–52.
Hall, A., 1996. Igneous Petrology. Longman, London, p. 551.
Hastie, A.R., Kerr, A.C., 2010. Mantle plume or slab window? Physical and geochemical constraints on the origin of the Caribbean oceanic plateau. Earth-Science Reviews 98, 283–293.
Herzberg, C., Asimow, P.D., 2008. Petrology of some oceanic island basalts: PRIMELT2.XLS software for primary magma calculation. Geochemistry, Geophysics, Geosystems 9, Q09001. http://dx.doi.org/10.1029/2008GC002057.
Herzberg, C.T., Zhang, J., 1996. Melting experiments on anhydrous peridotite KLB-1: compositions of magmas in the upper mantle and transition zone. Journal of Geophysical Research 101, 8271–8295.
Herzberg, C., Asimow, P.D., Arndt, N., Niu, Y., Lesher, C.M., Fitton, J.G., Cheadle, M.J., Saunders, A.D., 2007. Temperatures in ambient mantle and plumes: constraints from basalts, picrites, and komatiites. Geochemistry, Geophysics, Geosystems 8, Q02006. http://dx.doi.org/10.1029/2006GC001390.
Jaffarian, A., Emami, H., Vousughi Abedini, M., Ghaderi, M., 2009. Petrology and Geochemistry of Lower Paleozoic Magmatism in the East of Alborz. PhD thesis. Islamic Azad University of Sabzevar, p. 298 (in Persian).
Jung, C., Jung, S., Hoffer, E., Berndt, J., 2006. Petrogenesis of tertiary mafic alkaline magmas in the Hocheifel, Germany. Journal of Petrology 47, 1637–1671.
Kristan-Tollmann, E., Tollmann, A., Halnedani, A., 1979. Beitraige zur Kenntnis der Trias yon Persien. I. Revision der Triasgliederung, Rhfit fazies im raum yon Isfahan und Kossener Fazieseinschlag bet Waliabad SE Abadeh. Wien. Mitteilungen der Österreichische Mineralogische Gesellschaft 70, 119–186 (in German).
Leake, B.E., Woolley, A.R., Arps, C.E.S., 1997. Nomenclature of amphiboles: report of the subcommittee on amphiboles of the International Mineralogical Association Commission on new minerals and mineral names. Mineralogical Magazine 61, 295–321.
Leoni, L., Saitta, M., 1975. X-ray fluorescence analysis of 29 trace elements in rocks and mineral standards. Rendiconti Soc. Italiana di Mineralogia e Petrologia 32, 497–510.
Lustrino, M., Carminati, E., 2007. Phantom Plumes in Europe and the Circum-Mediterranean Region. The Geological Society of America, Special Paper 430. http://dx.doi.org/10.1130/2007.2430(33).
Machado, A., Lima, E.F., Chemale, J.F., Morata, D., Oteiza, O., Almeida, D.P.M., Figueiredo, A.M.G., Alexandre, F.M., Urrutia, J.L., 2005. Geochemistry constraints of Mesozoic–Cenozoic calc-alkaline magmatism in the South Shetland arc, Antarctica. Journal of South American Earth Sciences 18, 407–425.
McBirney, A.R., 2006. Igneous Petrology, third ed. Jones and Bartlett, Sudbury, MA, p. 550.
McDonough, W.F., Sun, S.S., 1995. Composition of the Earth. Chemical Geology 120, 223–253.
McKenzie, D.P., Bickle, M.J., 1988. The volume and composition of melt generated by extension of the lithospheric. Journal of Petrology 29, 625–679.
McKenzie, D., O'Nions, R.K., 1991. Partial melt distributions from inversion of rare earth element concentrations. Journal of Petrology 32, 1021–1091.
McKenzie, D., O'Nions, R.K., 1995. The source regions of oceanic island basalts. Journal of Petrology 36, 133–159.
Mertz, D.F., Weinrich, A.J., Sharp, W., Renne, P.R., 2001. Alkaline intrusions in a near-treanch setting, Franciscan complex, California: constraints from geochemistry, petrology and $^{40}Ar/^{39}Ar$ chronology. American Journal of Science 301, 877–911.
Mirnejad, H., Hassanzadeh, J., Cousens, B.L., Taylor, B.E., 2010. Geochemical evidence for deep mantle melting and lithospheric delamination as the origin of the inland Damavand volcanic rocks of northern Iran. Journal of Volcanology and Geothermal Research 198, 288–296.
Morimoto, N., Fabries, J., Fergusson, A.K., Guizbourg, I.D., Ross, M., Seifert, F.A., Zussman, J., Aoki, K., Gottardi, G., 1988. Nomenclature of pyroxenes. American Mineralogist 173, 1123–1133.
Nabavi, M.H., Seyed emami, K., 1977. Sinemurian ammonites from the Shemshak Formation of the north Iran (Semnan area. Alborz). Neues Jahrbuch für Geologie und Paläontologie Abhandlungen 153, 70–85.
Nazari, H., Shahidi, A., 2011. Tectonic of Iran «Alborz». Geological Survey and Mineral Exploration of Iran. Research Institute for Earth Science, p. 97.
Nazari, H., Omrani, J., Shahidi, A.R., 2004. Geological Map of Anzali, Scale 1:100000. Geological Survey of Iran.
Peters, T.J., Menzies, M., Thitlwall, M., Kyle, P.K., 2008. Zuni-Bandera volcanism, Rio Grande, USA–Melt formation in garnet- and spine-facies mantle straddling the asthenosphere–lithosphere boundary. Lithos 102, 295–315.
Haghnazar, Sh, Vousughi Abedini, M., Poor Moafi, M., 2009. Petrology and Geochemistry of Mafic Rock in Javaher Dasht Area, East of Gillan Province, North of Iran. PhD thesis. Shahid Beheshti University, p. 298.
Pouchou, J.L., Pichoir, F., 1984. Un nouveau modèle de calcul pour la microanalise quantitative par spectrométrie de rayon-X: I. Application à l'analyse d'échantillons homogènes. La Recherche Aérospatiale 3, 167–192 (in France).
Putirka, K.D., Perfit, M., Ryerson, F.J., Jackson, M.G., 2007. Ambient and excess mantle temperatures, olivine thermometry, and active vs. passive upwelling. Chemical Geology 241, 177–206. http://dx.doi.org/10.1016/j.chemgeo.2007.01.014.
Rollinson, H., 1998. Using Geochemical Data: Evaluation, Presentation, Interpretation. Longman Scientific and Technical, p. 352.
Sabzehei, M., 1993. Calendrier de la migration permo-triasique et morcellement mésozoique des éléments continentauz de l Iran. PhD thése. Université Pierre et Marie Curie, Paris, France, p. 298 (in French).
Sengör, A.M.C., 1990. A new model for the late Paleozoic- Mesozoic tectonic evolution of Iran and implications for Oman. In: Searle, M.P., Ries, A.C. (Eds.), The

Geology and Tectonics of the Oman Region. Geological Society of London Special Publication, pp. 797–831.
Sengör, A.M.C., Natal'in, B.A., 1996. Paleotectonics of Asia: fragments of a synthesis. In: Yin, A., Harrison, M. (Eds.), The Tectonic Evolution of Asia. Cambridge University Press, Cambridge, pp. 486–640.
Sengör, A.M.C., Altiner, D., Cin, A., Ustaomer, T., Hsu, K.J., 1988. Origin and assembly of the tethyside orogenic collage at the expense of Gondwana land. In: Audley-Charles, M.G., Hallman, A. (Eds.), Gondwana and Tethys, 37. Geological Society of London Special Publication, pp. 119–181.
Seyed emami, K., 2003. Triassic in Iran. Facies 48, 91–196.
Shahidi, A., 2005. Evolution tectonique et géodynamique des chaines de l Alborz et du Kopet-Dagh (Iran) depuise le Mésozoique. Journées des Doctorants, 3 et 4 mai, Ecole des Mines de Paris (in French).
Shahidi, A., 2008. Evolution tectonique du Nord de L Iran (Alborz et Kopet-Dagh) depuis le Mésozoique. PhD Thése. Université Pierre et Marie Curie, Paris, p. 500 (in French).
Shaw, D.M., 1970. Trace element fractionation during anatexis. Geochimica et Cosmochimica Acta 34, 237–243.
Smith, E.I., Sánchez, A., Walker, J.D., Wang, K., 1999. Geochemistry of mafic magmas in the Hurricane Volcanic Field, Utah: implications for small- and large scale chemical variability of the lithospheric mantle. Journal of Geology 107, 433–448.
Sodoudi, F., Yuan, X., Kind, R., Heit, B., Sadidkhouy, A., 2009. Evidence for a missing crustal root and a thin lithosphere beneath the Central Alborz by receiver function studies. Geophysics Journal International 177, 733–742.
Soffel, H.C., Förster, H.G., 1984. Polar wander path of the Central-East-Iran microplate including new results. Neues Jahrbuch fur Geologie und palaontologie, Abhandlungen 168, 165–172.
Stampfli, G.M., 1996. The Intra-Alpine terrain: a Paleotethyan remnant in the alpine variscides. Eclogae Geologicae Helvetiae 89, 13–42.
Stampfli, G.M., 2000. Tethyan oceans. In: Bozkurt, E., Winchester, J.A., Piper, J.D.A. (Eds.), Tectonics and Magmatism in Turkey and Surrounding Area, 173. Geological Society of London, Special Publication, pp. 163–185.
Stampfli, G.M., Marcoux, J., Baud, A., 1991. Tethyan margins in space and time. Palaeogeography, Palaeoclimatology, Palaeoecology 87, 373–409.
Steiger, R., 1966. Die geologie der west-Firuzkuh area (Zentralelburz/Iran). Mitteilungen aus dem Geologischen Institut der Eidgen6ssischen Technischen Hochschule und der Universitiit Zurich, p. 145 (in German).
Stocklin, J., 1974. Northern Iran: alborz mountains. In: Spencer, A.M. (Ed.), Mesozoic–Cenozoic Orogenic Belts; Data for Orogenic Studies; Alpine-Himalayan Orogens, 4. Geological Society of London Special Publication, pp. 213–234.
Sussli, P.E., 1976. The Geology of the Lower Haraz Valley Area, Central Alborz, Iran. Geological Survey of Iran, p. l16.
Taraz, H., 1974. Geology of the Surmaq-dehbid Area, Abadeh Region, Central Iran. Internal report, 138. Geological Survey of Iran, Tehran, pp. 1–37.
Taylor, S.R., McLennan, S.M., 1985. The Continental Crust: its Composition and Evolution. Blackwell Scientific, Oxford, p. 312.
Thirlwall, M.F., Smith, T.E., Graham, A.M., Theodorou, N., Hollings, P., Davidson, J.P., Arculus, R.J., 1994. High field strength element anomalies in arc lavas: source or process? Journal of Petrology 35, 819–838.
Vahdati Daneshmand, F., Nadim, H., 2001. Geological map of Marzanabad quadrangle. Geological Survey of Iran. Quadrangle map scale, 1/100000.
Völlmer, T., 1987. Zur Geologie des nordlichen Zentral-elburz zwischen Chalus-und Haraz-Tal. Iran. Mitteliungen aus dem Geologisch-Palaontologischen, 63. Institut der Universitat Hamburg, pp. 1–125 (in German).
Wang, Y.J., Fan, W.M., Zhang, H.F., Peng, T.P., 2006. Early cretaceous gabbroic rocks from the Taihang mountains: implications for a paleosubduction-related lithospheric mantle beneath the central North China Craton. Lithos 86, 281–302.
Wass, S.Y., 1979. Multiple origins of clinopyroxene in alkalic basaltic rock. Lithos 12, 115–132.
White, R.S., McKenzie, D., 1989. Magmatism at rift zones: the generation of volcanic continental margins and flood basalts. Journal of Geophysical Research: Solid Earth 94, 7685–7729.
Wilkinson, J.F.G., 1974. Garnet clinopyroxenite inclusions from diatremes in the Gloucester area, New South Wales. Contributions to Mineralogy and Petrology 46, 275–299.
Wilson, M., 1989. Igneous Petrogenesis a Global Tectonical Approach. Chapman and Hall, p. 466.
Wilson, M., Downes, H., 1991. Tertiary Quaternary extension-related alkaline in western and central Europe. Journal of Petrology 32, 811–849.
Winchester, J.A., Floyd, P.A., 1977. Geochemical discrimination of different magma series and their differentiation products using immobile elements. Chemical Geology 20, 325–343.
Wlodyka, R., 2002. Clinopyroxene and Amphibole Zoning Patterns in Teschnite Rocks from the Outer Western Polish Carpatians. Congress of Carpatian-Balkan geological association Bratislava. September 1st–4th.
Wörner, G., 1999. Lithospheric dynamics and mantle sources of alkaline magmatism of the Cenozoic West Antarctic Rift System. Global and Planetary Change 23, 61–77.
Zanchi, A., Berra, F., Mattei, M., Ghassemi, M., Sabouri, J., 2006. Inversion tectonics in central Alborz, Iran. Journal of Structural Geology 28, 2023–2037.